COMMUNICATIONS CHEMISTRY

Corrected: Author Correction

ARTICLE

https://doi.org/10.1038/s42004-019-0141-4 OPEN

Understanding zeolite deactivation by sulfur poisoning during direct olefin upgrading

Jonathan H. Harrhy [1], Aiguo Wang[1], Jack S. Jarvis[1], Peng He [1], Shijun Meng[1], Matthew Yung[2], Lijia Liu[3] & Hua Song [1]

The presence of sulfur contaminants in bitumen derived crude oils can lead to rapid catalyst deactivation and is a major problem faced by downstream refiners. Whilst expensive hydrotreating steps may remove much of the sulfur content, it is important to understand how catalyst deactivation by sulfur poisoning occurs and how it may be mitigated. Here we report a mechanistic study of sulfur poisoning over a zeolite catalyst promoted with silver and gallium Lewis acids. Olefin upgrading, an essential process in the refinement of heavy oils, is used as a model reaction. Access to the zeolite inner pores is blocked by bulky, weakly adsorbed sulfur species. Pore access and thus catalyst activity is restored by increasing the reaction temperature. We also show that a simple alkaline treatment greatly improves both the sulfur tolerance and performance of the catalyst. These findings may enhance the rational design of heterogenous catalysts for olefin upgrading.

[1] Department of Chemical and Petroleum Engineering, University of Calgary, Calgary T2N 1N4 AB, Canada. [2] National Bioenergy Center, National Renewable Energy Laboratory, 15013 Denver West Parkway, Golden, CO 80401, USA. [3] Jiangsu Key Laboratory for Carbon-Based Functional Materials & Devices, Institute of Functional Nano and Soft Materials (FUNSOM), Soochow University-Western University Centre for Synchrotron Radiation Research, Soochow University, Suzhou, Jiangsu 215123, China. Correspondence and requests for materials should be addressed to H.S. (email: sonh@ucalgary.ca)

Depletion of conventional oil sources has led to a surge in demand for feasible alternatives. Therefore, unconventional crude oils such as bitumen have attracted much attention in recent years. Reserves of bitumen oil sands were estimated to be 24 billion barrels at the end of 2015 in Canada alone (retrieved from: https://www.aer.ca/providing-information/data-and-reports/statistical-reports/st98). The viscosity and density of heavy crude oils necessitates partial upgrading via high temperature cracking prior to transportation to refineries downstream. However, the partial upgrading of heavy oils leads to the formation of high quantities of olefinic compounds as by-product. The chemical instability and high concentration of olefins in partially upgraded streams can lead to the formation of highly undesirable polymeric deposits following prolonged periods in storage or during long distance pipeline transportation[1].

A major problem faced by refiners is the sulfur content of heavy hydrocarbon feeds such as bitumen-derived heavy oils and product streams such as delayed coker light naphtha[2]. Reducing sulfur contaminants is of vital importance as unconverted sulfur poisons may not only lead to rapid deactivation of zeolitic catalysts for downstream refining[3] but also contribute towards the production of harmful SO_x emissions. Sulfur content has been strongly correlated to the olefin content in such feeds[4]. Therefore, it is desirable to produce a heterogeneous catalyst that is not only active for the selective upgrading of olefins, but that is also resistant to deactivation via sulfur species.

Perhaps the most well-known class of catalytic materials for oil upgrading are zeolites. Zeolite catalysts, such as HZSM-5, have also displayed promising activity towards the selective upgrading of olefins. Modification with metal dopants such as gallium (Ga) can increase activity and promote increased yields of valuable aromatic products[5]. However, the high temperatures typically employed industrially often result in significant coke formation, although the thermal stability of ZSM-5 catalysts may be enhanced by modifications such as phosphorous addition[6, 7] and alkaline treatment[8].

A common theme throughout the literature is the use of hydrogen gas for refining processes, despite the natural unavailability and cost of H_2, which are severe drawbacks to hydrotreatments. It is well known that H_2 is mainly produced via catalytic steam reforming of methane, yielding syngas[9]. We have previously shown that by employing a HZSM-5 catalyst loaded with silver (Ag)[10, 11], gallium (Ga)[10, 11], palladium (Pd)[12–14] and iridium (Ir)[14, 15], olefin feedstocks may be directly upgraded to paraffins, naphthenes and aromatics under CH_4 environment[10].

Herein, we report the effect of sulfur contaminants on the catalytic direct upgrading of olefins using a Ag-Ga/ZSM-5 zeolite catalyst. It is found that sulfur poisoning is temporary and occurs only when sulfur species are present in the reaction medium. Catalyst poisoning is shown to be significant in the presence of bulky sulfur molecules such as dibenzothiophene (DBT), which inhibits access to the zeolite micropores by weakly adsorbing to Ag and Ga species located on the external surface, preventing key steps from occurring in the olefin upgrading reaction. Sulfur poisoning is shown to be temperature-dependent and full catalyst activity is recovered upon increasing reaction temperature to 400 °C. We also show that catalyst performance and sulfur poisoning are mitigated by introducing mesoporosity into the catalyst through a simple post-synthetic alkaline treatment.

Results

Direct olefin upgrading with a simulated feed. Initial investigations with a simulated feed (composition given in Supplementary Table 1) yields an 83 wt% olefin reduction with high selectivity towards aromatics (Supplementary Fig. 1). Adding 5 wt% diethyl sulfide (DES) and DBT to the reaction mixture (sulfur to metal ratio of 1:0.001 for both Ag and Ga metals) represses both olefin reduction and aromatic formation. Interestingly, catalyst activity is recovered upon removal of sulfur from the reaction medium and Ag-Ga/ZSM-5 is only temporarily and partially deactivated by sulfur.

1-Decene model compound studies. The deactivation mechanism was probed using 1-decene as a model compound. The reader is directed to Supplementary Tables 2–6 for major products of the reactions discussed below and Supplementary Note 1 for the equations used for performance evaluation. Fig. 1a shows that at 330 °C, olefin reduction is relatively low (35 wt%) compared to the simulated feed (80 wt%), likely due to the lower olefin content and co-reactants present. Olefin reduction increases as a function of temperature, with values of 35 wt% and 91 wt% achieved at 330 and 400 °C, respectively. Fig. 1b displays the relationship between reaction temperature and selectivity towards both paraffins and aromatics. At 330 °C, paraffins are the major products, with concentrations of 9 wt% and 22 wt% of aromatics and paraffins observed in the product oil, respectively. Increasing reaction temperature promotes aromatic formation until it plateaus at 400 °C (71 wt%). Analogous reactions were then run with DBT and DES contaminants present. Olefin reduction is essentially switched off at 330 °C (Fig. 1c), however, sulfur poisoning is diminished with increasing temperature and is negligible at 400 °C. The extent of catalyst deactivation at 330 °C was investigated via reuse with fresh 1-decene. As with the simulated oil feed discussed earlier, catalyst activity is almost entirely recovered, with olefin reductions of 35 wt% and 30 wt% for fresh and reused catalyst, respectively (Fig. 1e). We conclude that for direct olefin upgrading over Ag-Ga/ZSM-5, sulfur deactivation is only temporary and, furthermore, is only observed when sulfur contaminants are directly present in the reaction medium. This may suggest that DBT and DES contaminants desorb from key active sites for olefin transformation, particularly into aromatics, as reaction temperature increases from 330 to 400 °C.

Shorter reaction times of 10–30 min were then performed and additionally, the extent of olefin reduction that occurs during the heat-up phase of the reaction was investigated. This was achieved by allowing the reaction to reach the desired temperature at the normal heating rate and once at the desired temperature, the reaction was immediately quenched by submerging the vessel into an ice bath. Complete sulfur deactivation was observed even after 10 min at 330 °C, demonstrating that Ag-Ga/ZSM-5 deactivation via sulfur poisoning is rapid (Supplementary Table 7). On increasing the temperature, the reaction proceeds quickly, with >60 wt% olefin reduction seen during the heat-up phase to 400 °C both in the presence and absence of sulfur (Supplementary Fig. 2).

Our initial results with a simulated oil feed indicate that co-reactants may strongly influence not only the olefin upgrading activity of the catalyst but also deactivation due to sulfur contaminants. Olefin upgrading experiments were therefore performed using heptane and benzene as model paraffin and aromatic co-reactants, respectively. Paraffin co-reactant plays no positive role during direct olefin upgrading at 330 °C, whereas aromatic co-reactant may improve olefin reduction by promoting aromatic alkylation reaction between olefin substrate and aromatic co-reactant over Ag-Ga/ZSM-5 (Supplementary Fig. 3 and Supplementary Table 8). Furthermore, aromatics may react with organosulfur contaminants to form alkylbenzene products, inhibiting catalyst deactivation[16]. The reader is directed to Supplementary Discussion for a more detailed analysis.

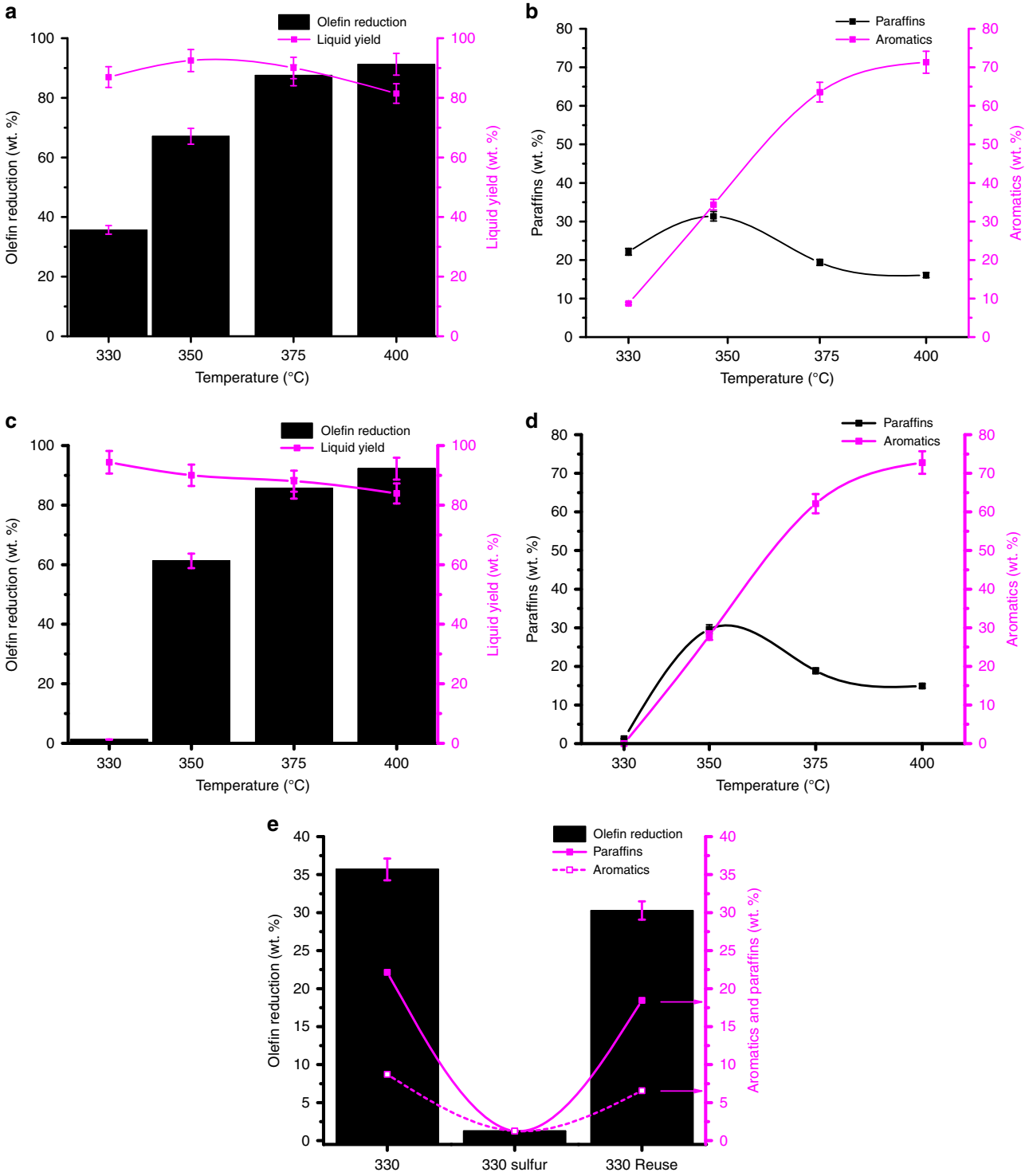

Fig. 1 Olefin reduction over Ag-Ga/ZSM-5 at various temperatures and times. **a** Olefin reduction performance at varying temperatures using 1-decene as substrate. Black bars indicate olefin reduction and magenta squares indicate liquid yield. **b** Selectivity towards paraffins and aromatics in product oil using 1-decene as substrate. Magenta squares indicate aromatics and black squares indicate paraffins. **c** Olefin reduction at varying temperatures using 1-decene as substrate in the presence of DBT and DES. Black bars indicate olefin reduction and magenta squares indicate liquid yield. **d** Selectivity towards paraffins and aromatics in product oil using 1-decene as substrate in the presence of DBT and DES. Magenta squares indicate aromatics and black squares indicate paraffins. **e** Olefin reduction performance of fresh, deactivated following reaction with DBT and DES and reused deactivated catalyst samples at reaction temperature of 330 °C. Black bars indicate olefin reduction and solid magenta line with magenta shaded squares indicates selectivity towards paraffins, dashed magenta line with magenta hollow squares indicates selectivity towards aromatics. All error bars represent ±4% calculated as standard deviation

Catalyst characterisation. Both fresh and 1-decene spent catalysts were characterised via X-ray photoelectron spectroscopy (XPS), high-resolution transmission electron microscopy (HR-TEM), diffuse reflectance infrared fourier transform spectroscopy (DRIFT) and NH_3 temperature programmed desorption (NH_3-TPD) (Supplementary Figs. 4–8 and Supplementary Table 9). Characterisation of fresh and 1-decene spent Ag-Ga/ZSM-5 agrees with our previous studies on this catalyst[11, 17]. The reader is directed to Supplementary Discussion for in-depth discussion and results.

The effects of DES and DBT contaminants on the catalyst properties were investigated by characterising spent Ag-Ga/ZSM-5 samples following reaction with 1-decene and sulfur contaminants at both 330 and 400 °C. XPS analysis of spent samples exposed to sulfur contaminants shows significant differences in both the Ag $3d_{5/2}$ and Ga $2p_{3/2}$ regions. Fig. 2a shows peak shifts of 1.1 and 1.4 eV in the Ag $3d_{5/2}$ region of 330 °C and 400 °C spent samples, respectively. Furthermore, a small binding energy (B.E.) shift of 0.3 eV is seen between the spent samples, with peaks centred at 367.9 and 368.2 eV for 330 °C and 400 °C samples, respectively. Whilst both values have been attributed to Ag_2S[18], the reported values for Ag metal are similar and so absolute identification of the Ag species present is not possible solely from this data[19]. The Ga $2p_{3/2}$ region (Fig. 2b) shows a significant shift in B.E. from 1118.8 eV in the fresh catalyst to 1117.8 eV for both spent catalysts. The Ga $2p_{3/2}$ peak at 1117.8 eV has been attributed to α-Ga_2O_3[20], however, this may also be assigned to Ga_2S_3[21, 22], suggesting that Ga_2S_3 may be formed upon reaction with sulfur contaminants.

The surface concentration of gallium for spent samples appears to be decreased, indicating that some gallium species have migrated into the inner pores. Examination of the S 2*s* region reveals differences between the spent catalysts (Fig. 2c). The S 2*s* peak is centred at 226.4 eV following reaction at 330 °C, indicative of both Ag_2S and Ga_2S_3[23, 24]. Upon increasing reaction temperature to 400 °C, the S 2*s* peak shifts to 227.7 eV. An identical B.E. shift is assigned to the decomposition of Ag_2S to elemental sulfur elsewhere[23].

X-ray absorption near-edge structure (XANES) Ga *k*-edge spectra of Ag-Ga/ZSM-5 are shown in Supplementary Fig. 9. The reference spectrum of Ga_2O_3 shows an E_0 value of approximately 10,375 eV and a white line position of approximately 10,379 eV.

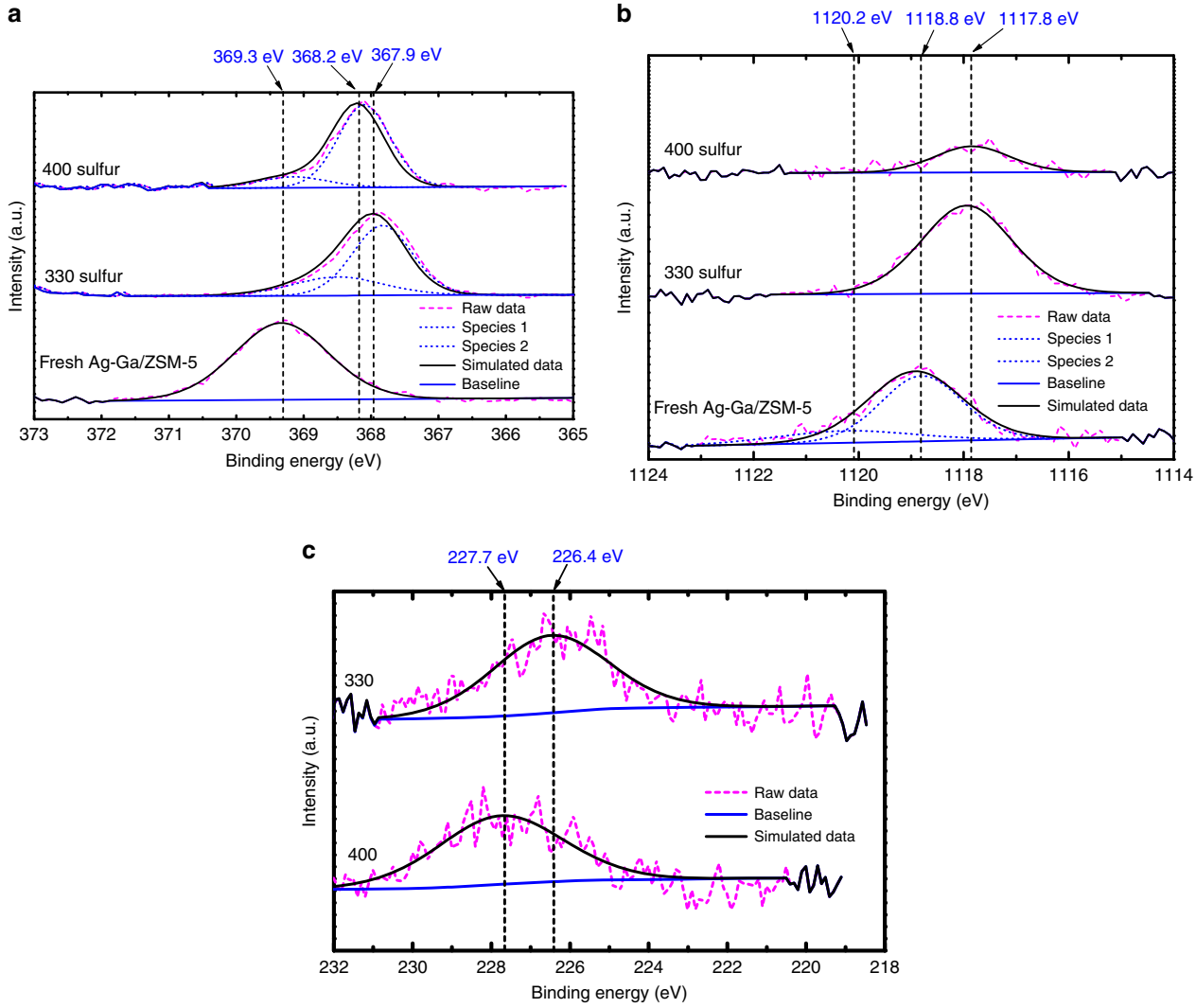

Fig. 2 XPS spectra of fresh and spent Ag-Ga/ZSM-5 catalyst samples. **a** Ag $3d_{5/2}$ region of fresh and spent Ag-Ga/ZSM-5 following reaction with 1-decene + DES + DBT at both 330 and 400 °C. **b** Ga $2p_{3/2}$ region of fresh and spent Ag-Ga/ZSM-5 following reaction with 1-decene + DES + DBT at both 330 and 400 °C. **c** S 2*s* region of spent Ag-Ga/ZSM-5 following reaction with 1-decene + DES + DBT at both 330 and 400 °C. For all spectra: solid black line indicates simulated (envelope) data, dotted blue lines indicate deconvoluted peaks, dashed magenta line indicates raw data and solid blue line indicates baseline

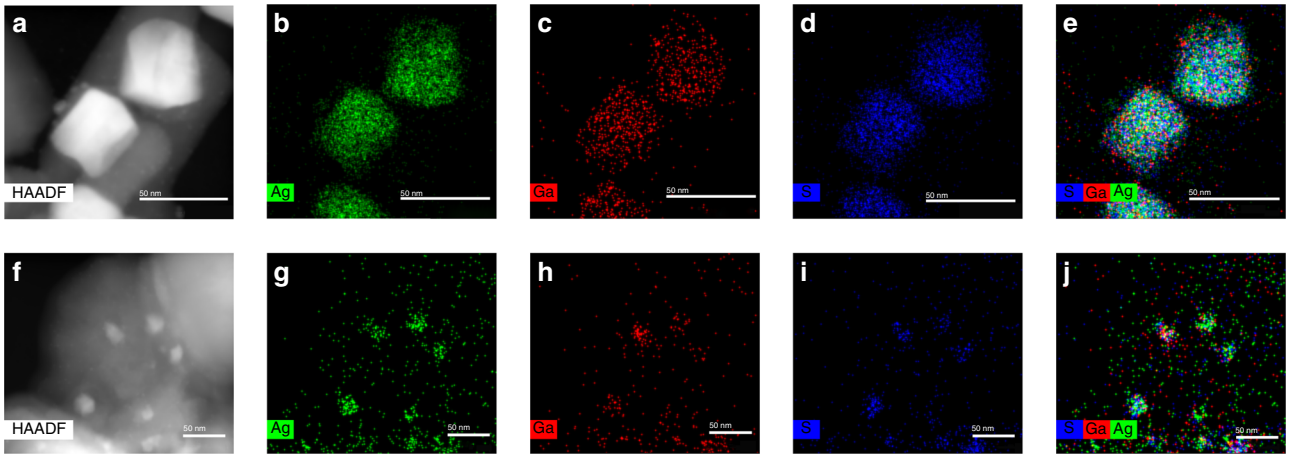

Fig. 3 TEM images and EMs of fresh and spent Ag-Ga/ZSM-5 catalyst samples. **a** high-angle annular dark field (HAADF) image of spent Ag-Ga/ZSM-5 following reaction with 1-decene + DES + DBT at 330 °C. **b**–**e** Ag, Ga, S and combined elemental mappings (EMs), respectively, of spent Ag-Ga/ZSM-5 following reaction with 1-decene + DES + DBT at 330 °C. **f** HAADF image of spent Ag-Ga/ZSM-5 following reaction with 1-decene + DES + DBT at 400 °C. **g**–**j** Ag, Ga, S and combined EMs, respectively, of spent Ag-Ga/ZSM-5 following reaction with 1-decene + DES + DBT at 400 °C. For all EMs: green indicates Ag, red indicates Ga and blue indicates S. Scale bars indicate 50 nm for all images

These values are proposed to correspond to tetrahedral (Ga_t) and octahedral (Ga_o) Ga^{3+} species, respectively[25, 26]. Upon exposure with 1-decene and sulfur contaminants, the E_0 position remains stable at approximately 10,375 eV, suggesting that there is no shift in the position of the Ga_t peak compared with the reference. However, the Ga_o peak appears to shift to approximately 10,378 eV during the heat-up phase and is shifted even further to 10,377 eV for all sulfur-exposed samples, evidenced by the shift in the white line position (Supplementary Table 10). Furthermore, the white line intensity decreases with increasing temperature. The observed changes to the Ga_o peak suggests that whilst much of the Ga^{3+} species remain in a tetrahedral coordination local environment, migration to the inner pores of the catalyst may also occur[27].

Spent, sulfur-exposed Ag-Ga/ZSM-5 samples were imaged using HR-TEM with elemental mapping (EM). Fig. 3a–e reveals that following reaction at 330 °C, sulfur species are bound to large agglomerates containing both Ag and Ga species, likely formed as a consequence of sintering, on the outer surface of the zeolite support i.e. not within the pores. Ag sintering is seemingly increased at 400 °C and surface sulfur species are primarily bound to these Ag clusters (Fig. 3f–j). It is known that the size of metal clusters may also affect the electronic affinity for sulfur adsorption on Ag particles[28]. Notably, the surface coverage of sulfur appears significantly reduced as the reaction temperature is increased to 400 °C, aligning with our experimental observations of recovered catalyst activity at higher reaction temperatures.

Acid site analysis of spent sulfur-exposed samples was performed using NH_3-TPD. Following reaction at 330 °C, two new peaks appear in the NH_3-TPD profile of Ag-Ga/ZSM-5 centred at approximately 370 °C and 415 °C (Fig. 4b), neither are indicative of the weak or strong acid sites seen on the fresh sample (Fig. 4a). Our TEM observations suggest that sulfur species are still present on this sample, principally bound to both Ag and Ga species on the external surface. It is plausible that NH_3 may therefore preferentially adsorb to these sulfur species yielding the differences in the NH_3-TPD profile of this sample compared with fresh Ag-Ga/ZSM-5. Only weak and medium acid sites are present on the 400 °C spent sample (Fig. 4c), in keeping with our previous findings that strong acid sites remain occupied post reaction[11]. The disappearance of the peaks at 370 °C and 415 °C upon increasing reaction temperature indicates that much of the sulfur species have desorbed from Ag-Ga/ZSM-5.

To further validate this, TPD experiments were performed on spent catalyst samples using He as carrier gas. Following reaction with sulfur poisons at 330 °C, two peaks are visible between approximately 350 and 500 °C in the TPD profile (Fig. 4d). Whereas, peaks are only observed in the much lower temperature range of approximately 100–320 °C for the 400 °C spent sample, implying that the active sites for olefin feed adsorption and transformation on the catalyst surface are temporarily blocked by sulfur poisons at low temperatures and become readily available again when reaction temperature is increased (e.g. >330 °C), probably due to decomposition and desorption. Quantification of acid sites reveals an increase for sulfur-exposed, spent samples (Supplementary Table 11) with values of 567, 1585 and 777 μmol NH_3 g^{-1} for fresh, spent 330 °C and spent 400 °C samples, respectively. These data further indicate that sulfur species capable of strongly adsorbing NH_3 are still present on all spent samples, but that significant desorption occurs at reaction temperatures >330 °C.

Additional TPD experiments were performed following adsorption of 1-decene, DBT and DES at room temperature. We note from the data shown in Fig. 4e that all samples show desorption peaks at temperatures attributed to weaker acid sites. Closer examination of the TPD profiles shows that following 1-decene adsorption, two weak, broad desorption peaks are observed at 200–400 °C. When DES and DBT are adsorbed on the catalyst, either alone or in a mixture with 1-decene, two distinct desorption peaks are seen at 200–350 °C and interestingly the intensity of these peaks is far greater compared to the desorption peaks seen following 1-decene adsorption alone. These data imply that sulfur contaminants, when present in the reaction medium, may strongly compete with 1-decene olefin substrate for adsorption upon weak and medium acid sites of Ag-Ga/ZSM-5 catalyst.

The strength of adsorption of DBT and DES on Ag-Ga/HZSM-5 was investigated using thermogravimetric analysis (TGA). DBT and DES were first adsorbed onto the catalyst surface and the resultant sample was subjected to TGA-DSC under N_2 flow, holding the temperature at 330 °C, where greatest catalyst deactivation due to sulfur poisoning occurs, before ramping to 500 °C. Supplementary Fig. 10 shows two sudden mass losses and

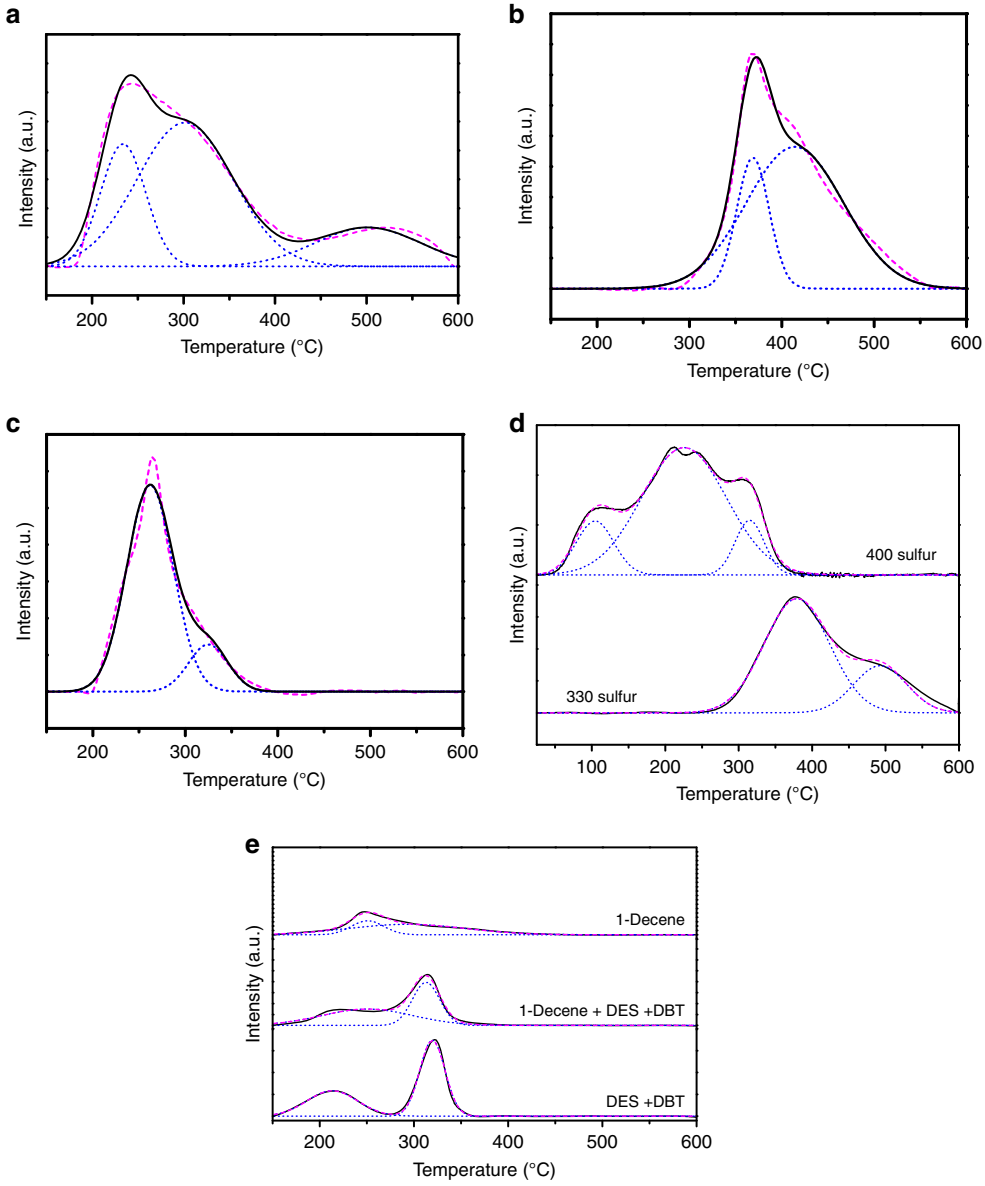

Fig. 4 NH_3-TPD and TPD profiles of fresh and spent catalyst samples. **a** NH_3-TPD profile of fresh Ag-Ga/ZSM-5. **b** NH_3-TPD profile of spent Ag-Ga/ZSM-5 following reaction with 1-decene + DBT + DES at 330 °C. **c** NH_3-TPD profile of spent Ag-Ga/ZSM-5 following reaction with 1-decene + DES + DBT at 400 °C. **d** TPD profile of spent Ag-Ga/ZSM-5 following reaction with 1-decene + DES + DBT at 330 and 400 °C. **e** TPD profiles of fresh Ag-Ga/ZSM-5 following adsorption at room temperature with: 1-decene, 1-decene + DBT + DES and DBS + DES. For all figures: solid black line indicates simulated data, blue dotted lines indicate deconvoluted peaks and magenta dashed line indicates raw data

exothermic heat flow at approximately 160 and 330 °C. The first peak centred at approximately 160 °C might indicate the decomposition of DES potentially chemically bonded to the catalyst surface, as this is significantly higher than the 98 °C boiling point of DES. The second sudden mass loss centred at approximately 330 °C corresponds with the boiling point of DBT indicating that DBT is weakly adsorbed on the catalyst surface. These data indicate that DES may desorb from Ag-Ga/ZSM-5 at relatively low temperatures whilst DBT remains adsorbed at temperatures <330 °C and may be chiefly responsible for observed Ag-Ga/ZSM-5 deactivation. Additionally, the decomposition of DES at temperatures >160 °C and the weakly chemisorbed nature of DBT may rationalise the restoration of the olefin reduction performance of spent Ag-Ga/ZSM-5 once it is charged in a sulfur-free medium. Our TGA data suggests that DBT desorbs from the surface of the spent catalyst at 330 °C. Therefore, when the spent catalyst is charged into a sulfur-free medium, desorption may occur from the surface at the reaction temperatures investigated (330–400 °C), thus freeing up the active sites for olefin upgrading.

Computational calculations. Density functional theory (DFT) calculations were performed to study the adsorption of DBT on the different surface acidic sites of Ag-Ga/ZSM-5. Four adsorption sites were selected: Al-OH, Si-OH, Ag atom and Ga atom. To calculate adsorption energy, a DBT molecule was placed around the aforementioned adsorption sites. Then, geometry optimisation was conducted to obtain the most stable structure. The adsorption energy of DBT was calculated based on Equation 7 (Supplementary Note 2). Images of the abovementioned structures are given in Supplementary Figs. 11–13.

Table 1 Theoretical calculation results obtained over Ag-Ga/ZSM-5 with DBT adsorbed on different sites

Adsorption sites	Adsorption energy (kJ mol^{-1})
Al-OH	−139.2
Si-OH	−136.6
Ag	−216.0
Ga	−216.9

The calculated adsorption energies are shown in Table 1. The adsorption energy of DBT on Al-OH and Si-OH are −139.2 kJ mol^{-1} and −136.6 kJ mol^{-1}, respectively. When DBT adsorbs on Ag or Ga atom, the adsorption energy was calculated at −216.0 kJ mol^{-1} and −216.9 kJ mol^{-1}, respectively. The increased negative adsorption energy of these metal sites suggests that DBT will preferentially adsorb on Ag and Ga species located on the external surface of Ag-Ga/ZSM-5. These data strongly agree with our XPS, TEM and TPD data and as such we tentatively conclude that DBT is mainly bound to Ag and Ga surface species during 1-decene upgrading reaction at 330 °C over Ag-Ga/ZSM-5. The calculated energies may also indicate the strength of adsorption of DBT over Ag-Ga/ZSM-5. The energies of physisorption and chemisorption of DBT over various sites of carbon nanotubes have been reported as 128.0–332.2 kJ mol^{-1} and 544.3–637.2 kJ mol^{-1}, respectively[29]. Our DFT calculations may therefore complement our TGA results, indicating that DBT only weakly interacts with the catalyst surface. Furthermore, these data may further rationalise the restoration of the olefin upgrading performance of Ag-Ga/ZSM-5 upon reuse at temperatures of 330 °C and above in a sulfur-free medium.

Influence of the zeolite structure. The mechanism of olefin aromatisation over zeolite catalysts is complex and multistep. More specifically, the formation of aromatics from n-C_7^+ olefins is reported to proceed via isomerisation, cracking, oligomerisation and finally hydrogen transfer[30]. Crucially, oligomerisation reactions have been shown to occur within the zeolite pores and, in blocking access to these pores as a result of high temperature coking, olefin conversion and aromatic formation is greatly suppressed[31]. Our characterisation data and computational studies suggest that DBT preferentially adsorbs upon Ag and Ga species located on the external surface of Ag-Ga/ZSM-5. Given the bulky size of DBT (kinetic diameter of approximately 9 Å)[32] relative to the micropores of ZSM-5 (pore limiting diameter of approximately 5.6 Å)[33] it may be blocking access to the inner pores when 1-decene upgrading is run at 330 °C, preventing olefin oligomerisation and cyclisation reactions and in turn, deactivating Ag-Ga/ZSM-5.

To explore this, we first calculated the selectivity towards diolefin and cycloolefin oligomers as a function of all olefins in the product oil. Fig. 5 shows that as reaction temperature increases, the selectivity towards cycloolefins increases whilst diolefin selectivity is decreased. Crucially, in the presence of DBT and DES, the formation of both cycloolefin and diolefin oligomers is inhibited at 330 °C, correlating with the deactivation of Ag-Ga/ZSM-5. The role of the porous structure of ZSM-5 can be investigated by comparing Ag-Ga/ZSM-5 with a Ag-Ga/SiO_2-Al_2O_3 catalyst with the same SiO_2:Al_2O_3 ratio. Fig. 6a shows that the activity is substantially worse over the mixed metal oxide catalyst, furthermore, aromatic formation is low and paraffins are the main product. Similarly, the effect of surface acidity was investigated by preparing a Ag-Ga/Si-MFI catalyst. Our data suggest that Brønsted acid sites may be vital for 1-decene upgrading to aromatics as essentially no olefin reduction and zero aromatic formation is seen following reaction at 400 °C over Ag-Ga/Si-MFI.

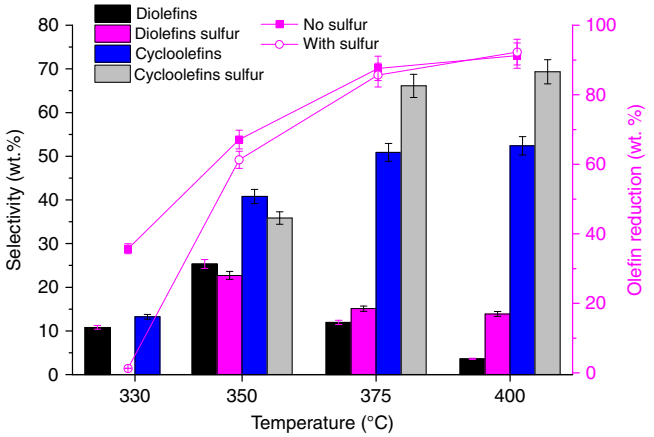

Fig. 5 Olefin reduction performance and selectivity towards various olefins in the product oil. Observed selectivity towards cycloolefins (blue bars indicate 1-decene only, grey bars indicate 1-decene + DBT + DES) and diolefins (black bars indicate 1-decene only, magenta bars indicate 1-decene + DBT + DES) as a function of all olefins remaining in product oil. Observed olefin reduction (shaded magenta squares indicate 1-decene only and hollow magenta circles indicate 1-decene + DBT + DES) over Ag-Ga/ZSM-5 at reaction temperature varying from 330 to 400 °C. All error bars represent ±4% calculated as standard deviation

The reaction mechanism was further probed by evaluating olefin distribution in the obtained product oils (Fig. 6b). Ag-Ga/Si-MFI yields predominantly linear monoolefins, whereas Ag-Ga/SiO_2-Al_2O_3 forms lighter, branched monoolefins, demonstrating that surface Brønsted acid sites are necessary for initial activation of 1-decene via isomerisation and subsequent cracking reactions. Comparing Ag-Ga/SiO_2-Al_2O_3 with bare HZSM-5 and Ag-Ga/ZSM-5, the role of Brønsted acid sites located within the zeolite pores becomes clear as oligomerisation reactions proceed on both zeolite catalysts forming cycloolefins and a small amount of diolefins.

The activation of olefins over solid acid catalysts is widely considered to occur through the formation of a carbenium ion following protonation of the C–C olefin double bond[34]. The exact nature of the carbenium ion is still a subject of debate within the literature and is thought to vary for double-bond isomerisation, skeletal isomerisation and cracking reactions[34–36]. Catalytic cracking of C_{6+} olefins is reported to involve β-scission of a tri-coordinated carbenium ion formed over Brønsted acid sites, yielding an olefin and a free, smaller carbenium ion[37]. In the presence of sulfur contaminants at 330 °C, negligible cracking activity occurs and 1-decene undergoes isomerisation, almost exclusively (Supplementary Fig. 14). In the absence of sulfur, cracking reactions proceed and many lighter, branched olefins are seen in the product oil. Prior to any appreciable cracking activity, C_{6+} olefins are reported to undergo multiple isomerisation reactions, meaning that they will rapidly adsorb and desorb from the catalyst surface many times before cracking[37]. Our data indicate that DBT may strongly inhibit cracking reactions and limit 1-decene isomerisation over Ag-Ga/ZSM-5 at 330 °C, which may be related to the reported requirement for multiple adsorption and desorption steps in the process.

Ag and Ga species are not thought to be involved in the isomerisation, cracking or oligomerisation reactions, evidenced by the inactivity of Ag-Ga/Si-MFI. Rather, Ag and Ga species are thought to actively catalyse dehydrogenation reactions promoting

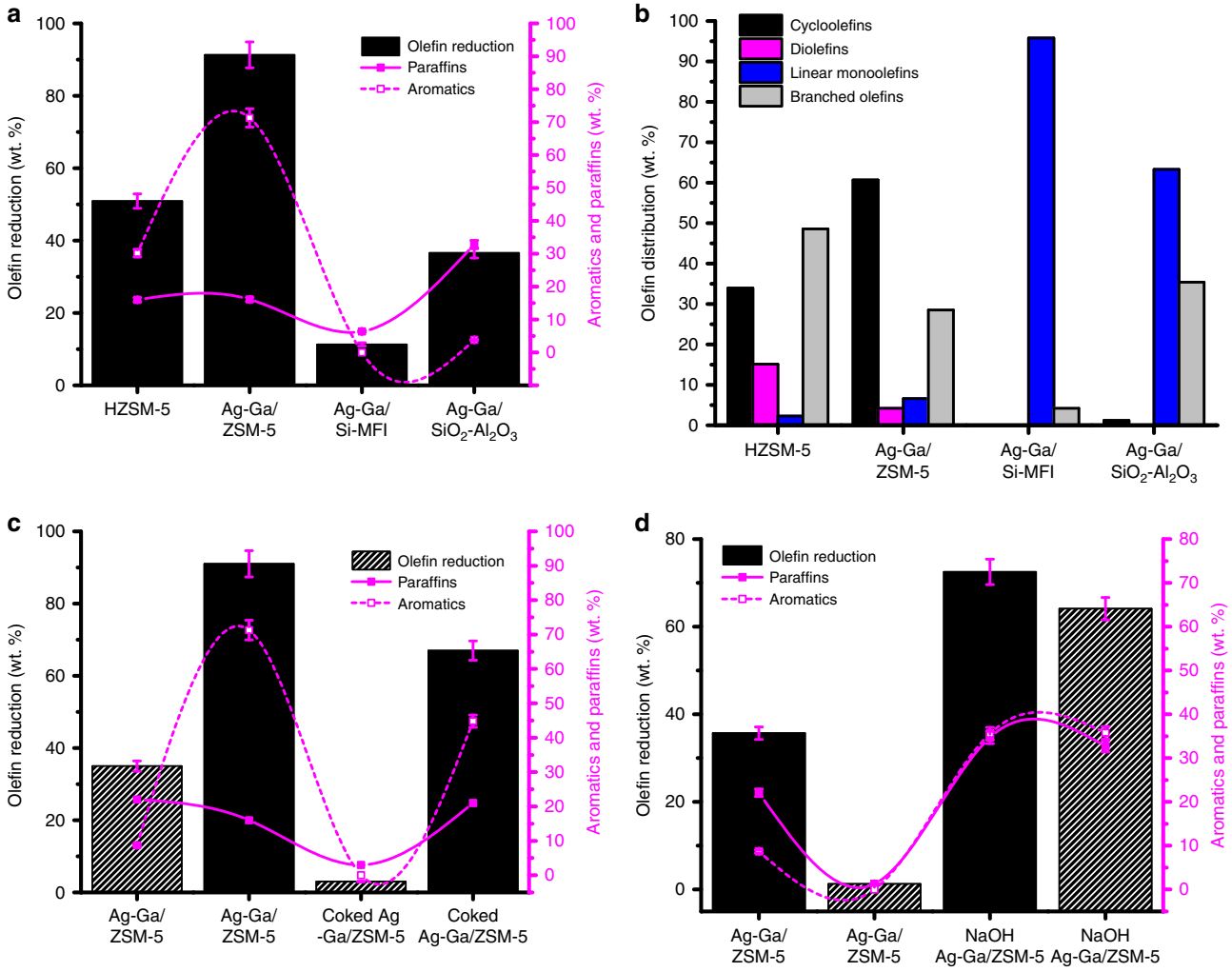

Fig. 6 Olefin reduction performance and olefin selectivity of various catalysts. **a** Olefin reduction performance of various catalysts at 400 °C using 1-decene as substrate. Black bars indicate olefin reduction, magenta solid line with magenta shaded squares indicates selectivity towards paraffins and magenta dashed line with magenta hollow squares indicates selectivity towards aromatics. **b** Distribution of olefins observed in the product oil over various catalysts using 1-decene as substrate at 400 °C, blue bars indicate linear monoolefins, grey bars indicate branched monoolefins, magenta bars indicate diolefins and black bars indicate cycloolefins. **c** Olefin reduction performance of Ag-Ga/ZSM-5 and coked Ag-Ga/ZSM-5 catalysts using 1-decene as substrate at 330 and 400 °C, black patterned bars indicate olefin reduction at 330 °C and black solid bars indicate olefin reduction at 400 °C. Magenta solid line with magenta shaded squares indicates selectivity towards paraffins, and magenta dashed line with magenta hollow squares indicates selectivity towards aromatics in product oil. **d** Olefin reduction performance of Ag-Ga/ZSM-5 and NaOH-treated Ag-Ga/ZSM-5 catalysts using 1-decene as substrate in the presence and absence of DBT and DES at 330 °C, black patterned bars indicate olefin reduction in the presence of DES and DBT, and black solid bars indicate olefin reduction in the absence of DES and DBT. Magenta solid line with magenta shaded squares indicates selectivity towards paraffins, and magenta dashed line with magenta hollow squares indicates selectivity towards aromatics in product oil. All error bars represent ±4% calculated as standard deviation

aromatic formation. These data are in good agreement with previous studies, which have concluded that Brønsted acid sites, located within the pores of the zeolite, are chiefly responsible for olefin oligomerisation and cyclisation whilst metal dopants such as Ga enhance the dehydrogenation of cycloolefin and diolefin intermediates[38, 39]. The relative rate of cycloolefin dehydrogenation is reported to be eight times that of linear and branched olefins over a Ga/ZSM-5 catalyst[40], and, if the formation of cycloolefins is inhibited then conversion to aromatics will likely not proceed. This aligns well with our experimental observations in the presence of sulfur. In summary, our data strongly suggest that adsorbed DBT inhibits the formation of olefin oligomers such as cycloolefins and furthermore that this reaction likely occurs within the zeolite pores.

Inner pore accessibility. To confirm the importance of inner pore accessibility in the upgrading of 1-decene, we performed a coking procedure known to selectively coke the inner pores of ZSM-5[17, 41]. When this coked Ag-Ga/ZSM-5 catalyst is employed for 1-decene upgrading at 330 °C, the catalyst activity is substantially diminished (Fig. 6c). Coking the inner pores of Ag-Ga/ZSM-5 prevents the formation of cycloolefins and diolefins, in keeping with our hypothesis that the inner pores are pivotal in the formation of these intermediates and therefore, aromatics. The textural properties of coked Ag-Ga/ZSM-5 was investigated by N_2 physisorption (Table 2). The coking procedure leads to a significant decrease in total surface area, from 491 m^2 $g^{-1}$to 266 m^2 g^{-1}. Micropore surface area was reduced by 46%, accompanied by a 50% reduction in micropore volume,

Table 2 N_2 physisorption data obtained over parent ZSM-5 support and various fresh, treated and spent Ag-Ga/ZSM-5 catalysts

Catalyst	BET surface area (m^2 g^{-1})	External surface area (m^2 g^{-1})	Micropore surface area (m^2 g^{-1})	Micropore volume (cm^3 g^{-1})
HZSM-5	485.1	81.0	404.1	0.17
Ag-Ga/ZSM-5	491.5	95.5	396.0	0.16
Coked Ag-Ga/ZSM-5	266.5	52.7	213.8	0.08
NaOH-treated Ag-Ga/ZSM-5	505.3	161.1	344.2	0.12
330 sulfur spent	220.6	41.8	178.8	0.07
400 sulfur spent	292.7	43.1	249.6	0.10

BET Brauner-Emmet-Teller

confirming that a significant amount of coke deposition occurs within the inner pores of Ag-Ga/ZSM-5.

Surface area analysis of spent, sulfur-exposed Ag-Ga/ZSM-5 shows interesting changes compared with fresh catalyst (Table 2). Brauner-Emmet-Teller (BET) surface area of the spent 330 °C sample decreased by 25% compared with the spent 400 °C sample, this is attributed almost exclusively to the microporous surface area. Micropore volume also decreased, with values of 0.07 cm^3 g^{-1} and 0.1 cm^3 g^{-1} for 330 °C and 400 °C spent samples, respectively. These data strongly indicate that access to the inner pores is hindered as a consequence of adsorbed species on the surface of Ag-Ga/ZSM-5 and that as the reaction temperature is increased, these species may desorb, resulting in a significantly increased microporous surface area and micropore volume.

Time of flight secondary ion mass spectroscopy (TOF-SIMS) shows a moderately intense peak at a *m*/*z* of 185 (Supplementary Fig. 15) in the spectrum of Ag-Ga/ZSM-5 following reaction with 1-decene and sulfur contaminants at 330 °C, which may be assigned to DBT (molecular mass = 184.26). The absence of this peak in the spectrum of all other samples may indicate that DBT presence on the surface of Ag-Ga/ZSM-5 is significant following reaction at 330 °C. Based upon all the above data, we tentatively conclude that DBT effectively blocks access to the inner pores of Ag-Ga/ZSM-5 at reaction temperature of 330 °C, preventing oligomerisation and aromatisation reactions from occurring and deactivating the catalyst.

Increasing the sulfur tolerance of Ag-Ga/ZSM-5. Simple post-synthetic treatments such as reaction with mild alkaline solutions have been shown to be highly effective in the transformation of conventional zeolites into hierarchical forms[42, 43]. Treatment of MFI-type zeolites with relatively mild concentrations of NaOH may effectively generate mesoporisity through the dissolution of framework silicon, whilst the framework aluminium and silicon neighbours are largely unaffected, preserving the Brønsted acidity to a good degree[44]. Such materials possess mesopores that are intricately connected with the characteristic zeolite micropores. Mesoporous zeolites have shown increased performance in the aromatisation of olefins due to enhanced micropore accessibility[8]. We therefore performed a simple alkaline treatment on Ag-Ga/ZSM-5 according to a method reported in the literature[45]. Interestingly, the alkaline treatment not only enhanced the olefin upgrading performance of Ag-Ga/ZSM-5 but also substantially mitigated the effects of sulfur poisoning. Fig. 6d shows that in the absence of sulfur, olefin reduction increases from approximately 35 wt% to approximately 73 wt% and, in the presence of sulfur, olefin reduction increases from 0 to approximately 64 wt%.

The textural properties of NaOH treated Ag-Ga/ZSM-5 are shown in Table 2. The external surface area increased significantly, from 95.5 m^2 g^{-1} to 161.1 m^2 g^{-1} following NaOH treatment, whereas the micropore volume decreased from

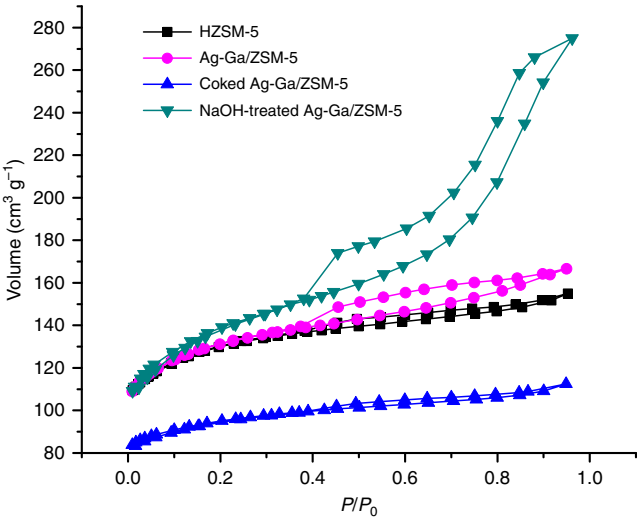

Fig. 7 Surface area analysis of fresh and spent catalysts. N_2 physisorption isotherms of parent ZSM-5 support and various fresh and treated Ag-Ga/ZSM-5 catalysts. Black squares indicate parent HZSM-5 support, magenta circles indicate fresh Ag-Ga/ZSM-5, blue triangles indicate coked Ag-Ga/ZSM-5 and turquoise triangles indicate NaOH modified Ag-Ga/ZSM-5

0.16 cm^3 g^{-1} to 0.14 cm^3 g^{-1} indicating that aluminium redistribution and amorphisation occurred during the treatment. A classic type IV isotherm with a characteristic hysteresis loop is present after NaOH treatment of Ag-Ga/ZSM-5, confirming the successful development of mesoporosity (Fig. 7)[43]. X-ray diffraction analysis shows that the MFI crystal structure of Ag-Ga/ZSM-5 is maintained following NaOH treatment (Supplementary Fig. 16).

The acidity of NaOH-modified Ag-Ga/ZSM-5 was analysed by pyridine DRIFT and NH_3-TPD. Although exact Lewis and Brønsted acid site quantification is not possible solely from our DRIFT spectra, as dictated by the Beer-Lambert Law, the signals obtained are shown as a function of absorbance to indicate any obvious changes in acid site distribution. Supplementary Fig. 17 shows that the area of the peak located at approximately 1540 cm^{-1}, assigned to pyridinium ion (Brønsted acid sites)[46, 47] relative to the area of the peak located at approximately 1450 cm^{-1} assigned to covalently bonded pyridine (Lewis acid sites)[46, 47] is diminished, indicating a relative increase in the number of Lewis acid sites. Quantification of NH_3-TPD curves (Supplementary Fig. 18 and Supplementary Table 12) reveals a slight decrease in the strong acid sites and a significant increase in the number of weak acid sites, consistent with the findings of others, suggesting an increase in Lewis acidity occurs following treatment of Ag-Ga/ZSM-5 with NaOH[45].

Such Lewis acid sites have been proposed to generate primarily at the mesoporous surface of ZSM-5 catalysts, rather than inside the micropores[45]. Our support control experiments have shown that the acid sites located inside the micropores of Ag-Ga/ZSM-5 are key for efficient transformation of olefin substrate into aromatics. Furthermore, our catalyst characterisations and computational analysis strongly suggest that DBT preferentially adsorbs upon Ag and Ga species located on the external surface of Ag-Ga/ZSM-5. Therefore, we reasonably assume that increased access to the micropores of Ag-Ga/ZSM-5 through the generation of a hierarchical mesoporous structure affects the olefin reduction performance of the catalyst and its resistance to sulfur poisoning via adsorbed DBT to a far greater extent than the generation of additional EfAl Lewis acid sites located primarily at the mesoporous surface. Consequently, the enhanced catalytic activity of NaOH-modified Ag-Ga/ZSM-5 in the presence of sulfur contaminants is reasonably assumed to be primarily due to the introduction of mesoporisity and a hierarchical structure.

Discussion

The introduction of Ag and Ga Lewis acid sites into microporous zeolite catalysts, such as ZSM-5 is known to increase dehydroaromatisation activity. Extraframework Ag^{+} Lewis acid sites are proposed to stabilise π-complexed intermediates, enhancing aromatic formation[48, 49]. Ga-promoted ZSM-5 catalysts are known to increase dehydrogenation activity towards olefin oligomers, significantly increasing aromatisation activity compared with their parent zeolite counterparts[31]. Whist evidence exists for methane incorporation over Ag and Ga modified zeolites, methane is not thought to play an active role in this study.

Ga-methoxy species, formed after methane activation, are reported to provide a route for incorporating methane into aromatic products[50]. Given that the formation of aromatics over Ag-Ga/ZSM-5 is blocked by sulfur poisoning at 330 °C, such a reaction pathway is proposed to not be relevant to the scope of this study. Nuclear magnetic resonance studies have shown that at reaction temperatures < 450 °C methane plays no active role in the transformation of olefins over Ag/HZSM-5 catalyst[49]. Furthermore, we have previously observed that under the reaction conditions investigated in this study, methane participation is negligible during the aromatisation of 1-decene, rather, methane participation was only seen when employing small olefin substrates over a Ag-Ga/ZSM-5 catalyst[11]. N_2 control experiments were performed to confirm the role of methane during 1-decene upgrading over Ag-Ga/ZSM-5. Supplementary Table 13 shows no appreciable difference in olefin upgrading performance under N_2 and CH_4 environments. On this basis, methane is not thought to play any noticeable role in this study.

Diolefin and cycloolefin formation is proposed to be the rate-limiting step in olefin aromatisation over Ga/ZSM-5 catalysts[40]. Once activated upon the external surface protonic acid sites of ZSM-5 catalysts, olefin oligomerisation and cyclisation steps occur within the inner pores of the zeolite, confirmed by our support material control experiments. We have shown through our catalyst characterisations and computational analysis that DBT may effectively bind to surface metal species sites such as Ag and Ga and, in doing so, can block the access to the inner pores of Ag-Ga/ZSM-5 due to its bulky size. Consequently, at a reaction temperature of 330 °C in a sulfur-containing reaction medium, the crucial oligomerisation of branched and linear monoolefins is prevented, resulting in little to no olefin reduction activity, this

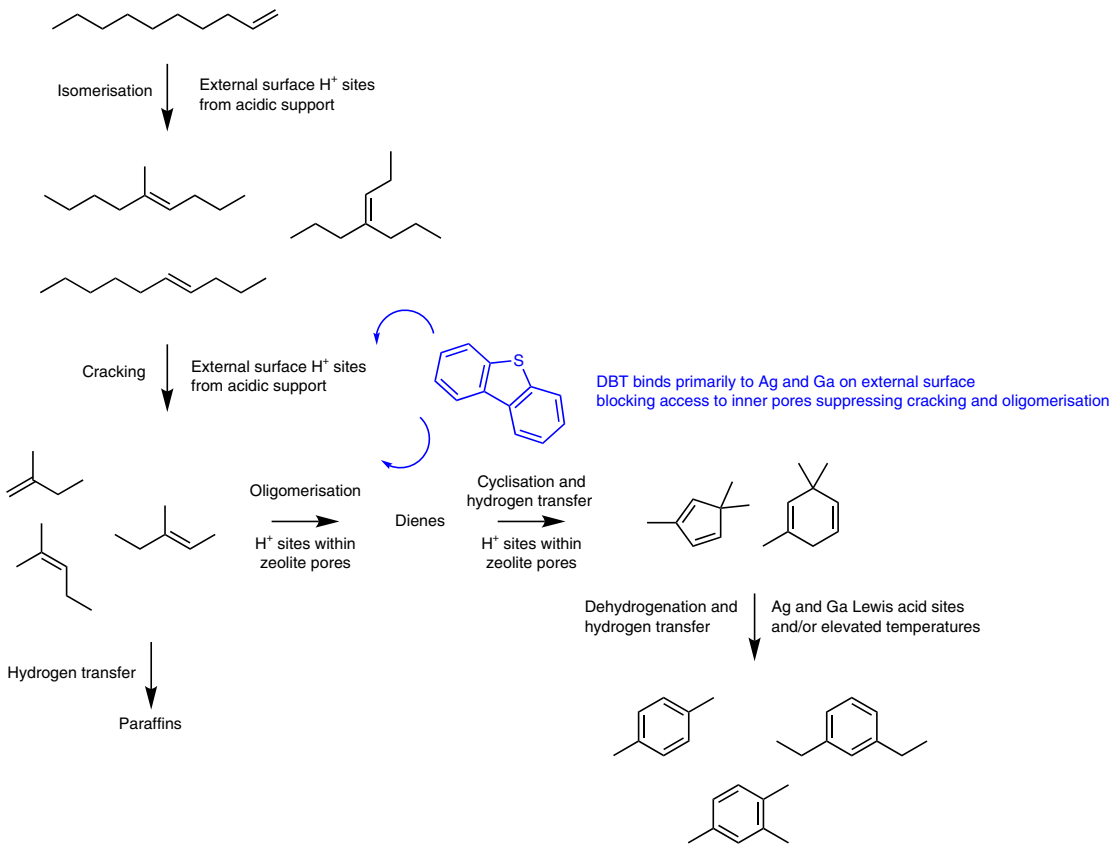

Fig. 8 Proposed sulfur deactivation mechanism. Proposed mechanism for the deactivation of Ag-Ga/ZSM-5 via sulfur poisoning with DBT contaminant during direct upgrading of 1-decene at 330 °C

deactivation pathway is summarised in Fig. 8. Upon increasing reaction temperature much of the adsorbed DBT is thought to desorb from Ag and Ga species on the external surface, enhancing access to the inner pores and restoring catalyst activity. Additionally, TGA analysis of sulfur-adsorbed Ag-Ga/ZSM-5 strongly indicates that DES may be effectively chemisorbed to the surface of the catalyst but will readily desorb and decompose at 160 °C and above, well below the reaction temperatures investigated in this study. Whereas DBT may be primarily weakly chemisorbed or physisorbed upon the surface of Ag-Ga/ZSM-5 and its desorption occurs at 330 °C and above. The temporary nature of sulfur deactivation and subsequent restoration of olefin upgrading activity is reasonably proposed to be due to the desorption of weakly adsorbed DBT from the surface of Ag-Ga/ZSM-5 once charged in a sulfur-free medium at reaction temperatures of 330 °C and above. Finally, we have also shown that in performing a simple NaOH treatment, mesoporosity may be introduced into Ag-Ga/ZSM-5, resulting in a greatly enhanced olefin reduction and aromatic formation during 1-decene upgrading at 330 °C and that deactivation by bulky sulfur poisons such as DBT may be almost entirely mitigated.

Methods

Catalyst preparation. Ammonium type ZSM-5 (NH_4-ZSM-5) obtained from Zeolyst, USA (CBV 8014) was converted to hydrogen type ZSM-5 (HZSM-5) by calcination in static air at 600 °C for 3 h. A silver- and gallium metal-modified HZSM-5 reported in our previous studies[11, 17] was prepared by wetness impregnation technique. In a typical synthesis, a certain amount of $AgNO_3$ (Sigma-Aldrich, 99.9+%) and $Ga(NO_3)_3{\cdot}xH_2O$ (Sigma-Aldrich, 99.9%+) were dissolved in 10 g deionised (DI) water to form an aqueous solution of metal precursors and HZSM-5 support was then impregnated with the metal precursor to give the desired metal weight loading. The obtained wet powder was first dried in an oven at 92 °C overnight, followed by calcination at 600 °C for 3 h in static air to give the final catalyst.

NaOH-treated Ag-Ga/ZSM-5 was prepared following the method described in the literature[45]. In a typical synthesis, HZSM-5 was treated in an aqueous 0.2 M NaOH (30 $cm^3\,g^{-1}_{zeolite}$) solution at 50 °C for 30 min under constant stirring. The obtained powder was ion exchanged three times by stirring in an aqueous 0.1 M NH_4NO_3 solution (100 $cm^3g^{-1}_{zeolite}$) for 12 h and converted to its protonic form via calcination in static air at 550 °C for 10 h (5 °C min^{-1} ramp rate). The desired amount of Ag and Ga metals was then loaded onto the obtained NaOH-treated catalyst as per the wetness impregnation method described earlier in this section followed by calcination at 600 °C for 3 h in static air.

Coked Ag-Ga/ZSM-5 was prepared using the method described in the literature[17, 41]. In a typical synthesis, NH_4-ZSM-5 was ion exchanged three times by stirring an aqueous 0.1 M $Ca(NO_3)_2{\cdot}4H_2O$ (Alfa Aesar, 99%) (100 $cm^3g^{-1}_{zeolite}$) at 80 °C and then calcined in static air at 550 °C for 2 h. The obtained powder was placed into a lab-fabricated flow reactor and treated at 600 °C under N_2 flow for 2 h followed by an ethylene/N_2 mixture for an additional hour. The obtained sample was ion exchanged three times by stirring in an aqueous 0.2 M NH_4NO_3 solution (100 $cm^3g^{-1}_{zeolite}$) at room temperature and converted into its protonic form via calcination under N_2 at 600 °C for 3 h. Finally, the desired amount of Ag and Ga metals was loaded onto the obtained coked catalyst as per the wetness impregnation method described earlier in this section followed by calcination at 600 °C for 3 h under N_2 environment.

SiO_2-Al_2O_3 mixed metal oxide support was prepared using tetraethyl orthosilicate (TEOS, 98%, Sigma-Aldrich) as the Si source and $Al(NO_3)_3{\cdot}9H_2O$ (99.9%, Alfa Aesar) as the Al source through co-precipitation using $NH_3{\cdot}H_2O$ as the alkaline agent. The molar ratio of SiO_2/Al_2O_3 was the same as the parent ZSM-5 support of Ag-Ga/ZSM-5. Ag-Ga/SiO_2-Al_2O_3 was then prepared as per the wetness impregnation method described earlier in this section followed by calcination at 600 °C for 3 h in static air.

SiO_2-MFI structure was prepared using hydrothermal synthesis method. A mixture of 22.66 g TEOS (98%, Sigma-Aldrich), 26.97 g Tetrapropylammonium hydroxide (TPAOH) (0.1 M, Sigma-Aldrich) and 22.65 g DI H_2O was stirred for 2 h at 300 rpm and then transferred in an autoclave and held at 180 °C for 3 days. The solid was recovered by centrifuge, dried and calcined at 550 °C for 3 h in static air. Ag-Ga/Si-MFI was then prepared as per the wetness impregnation method described earlier in this section followed by calcination at 600 °C for 3 h in static air.

Olefin upgrading reactions. Olefin upgrading tests were performed in a 300 mL batch reactor manufactured by Parr Instruments capable of tolerating high temperatures (up to 500 °C) and pressures (up to 14 MPa). In a typical reaction, 8.0 g of 1-decene (Alfa Aesar, 96%) and 0.08 g of Ag-Ga/HZSM-5 were placed into the reactor and purged with N_2 three times. The reactor was then charged with 1.0 MPa CH_4 and heated to the desired reaction temperature (330–400 °C) and held at reaction temperature for 1 h unless it is otherwise mentioned. Following reaction, the reactor was first ice cooled and then air cooled to room temperature. Once at room temperature, the liquid products were separated from solid catalyst via filtration. The resultant solid catalyst was then dried in a desiccator and either stored or recycled for reuse experiments. The liquid product oil composition was determined via analysis with a pre-calibrated gas chromatography mass spectrometer (GC-MS: PerkinElmer GC Claus 680 and MS Clarus SQ 8T) equipped with a paraffins-olefins-naphthenes-aromatics (PONA) column (Agilent HP-PONA). The oven temperature of the GC was programmed as follows: hold at 35 °C for 15 min, ramp at 1.5 °C min^{-1} to 70 °C, ramp at 3 °C min^{-1} to 150 °C and hold for 30 min, finally, ramp to 250 °C at 3 °C min^{-1} and hold for 2 min. Liquid products were divided into four major groups: paraffins, olefins, aromatics and naphthenes.

Sulfur impact reactions were performed in an identical manner to that described above, however, the reaction medium consisted of 1-decene (90 wt%) as substrate and DBT (5 wt%) (Sigma-Aldrich, 98%) and DES (5 wt%) (Sigma-Aldrich, 98%) as simulated sulfur contaminants. Experiments were also performed in an identical manner using a simulated oil consisting of heptane (Sigma-Aldrich, 99%), benzene (Sigma-Aldrich, 99.9%), 1-decene (Alfa Aesar, 96%), 2,2,4-trimethyl-1-pentene (Sigma-Aldrich, 99%), 1,5-hexadiene (Sigma-Aldrich, 97%) and cyclohexene (Alfa Aesar, 99%). Benzene and heptane were used to investigate the effect of co-reactants where the solution consisted of a 1:1 wt ratio, all other reaction conditions were kept identical to those described above. Reactions were all performed in triplicate and error bars were calculated to be ±4% based on standard deviation. Reaction performance was evaluated in terms of liquid and gas yield, olefin reduction and product distribution (see Supplementary Note 1).

Catalyst characterisation. XPS was performed using an AXIS-Ultra-DLD spectrometer (Kratos Analytical) using a mono-chromated Al Kα X-ray source (1486.6 eV). The XPS spectra of the selected elements were measured with a constant analyser pass energy of 80.0 eV. Calibration of all B.E.s was performed using the C 1*s* peak (B.E. = 284.6 eV).

HR-TEM was performed on FEI Talos F200X, a high-resolution scanning transmission electron microscope operated between 80 and 200 kV and equipped with high-angle annular dark field detector for Z contrast imaging and SuperX EDS detector for compositional analysis.

XANES measurements were performed at BL44A of the Taiwan Photon Source. This beamline is capable of acquiring quick XANES spectra at a speed of 500 ms per spectrum. A home-built reaction cell is installed at the beamline for in situ XANES measurement. All spectra were acquired in transmission mode. The reactant, composed of 90 wt% 1-decene, 5 wt% DES and 5 wt% DBT, was adsorbed on the catalyst pellet, which was put in the cell. The cell was purged by N_2 flow to remove the air in the cell. The cell was then sealed by closing the inlet and outlet valves. The temperature of the cell was controlled using an external heating system. The temperature was set from room temperature to 330 °C at the rate of 60 °C min^{-1}, and held at 330 °C for 5 min. It was ramped to 400 °C at a ramping rate of 20 °C min^{-1} and kept at 400 °C for 20 min. XANES spectra were collected every 500 ms throughout the course of reaction.

DRIFT was performed using a Thermo Scientific Nicolet iS50 equipped with environmental chamber and liquid-nitrogen cooled mercury–cadmium–telluride detector. The gas inlet of a multifunctional reactor system fabricated in our research laboratory was employed for the gas introduction to DRIFT via fluorinated ethylene propylene (FEP) tubing (Thermo Scientific, tubing 890 FEP, 8050–0125). The connection between the FEP tubing and the environmental chamber was accomplished through a short tubing with an inside diameter of 1/4 inch. The gas inlet was connected to a bubbler for liquid feedstock introduction via two three-way valves. Inlet gas could pass through the liquid sample before entering the chamber. First, the control group DRIFT spectra were acquired at 512 scans per spectrum with a resolution of 4 cm^{-1}. The catalyst was heated to 500 °C and held for 30 min under 30 sccm N_2 to remove the impurities, which might be adsorbed on the catalyst surface during storage. When the catalyst was cooled down to 25 °C the background spectrum was collected. Following background collections, a 30 sccm N_2 flow was introduced through the aforementioned bubbler filled with pyridine and kept for 20 min in order to introduce pyridine to the environmental chamber as the vapour phase. After that, the gas flow was switched back to 30 sccm pure N_2. The catalyst was held at 25 °C for 25 min before collecting sample DRIFT spectrum under transmission mode.

Surface acidity measurements were performed by NH_3-TPD using ~200 mg samples in an Altamira AMI-390 system. NH_3 was selected due to its simplicity, small molecular size and ability to titrate both strong and weak acid sites on the catalyst. Adsorption of NH_3 was performed using a flow of 30 sccm of 0.5% NH_3/N_2 for 90 min. After flowing He at 30 sccm for 1 h to remove any physically adsorbed NH_3, TPD was carried out by ramping to 600 °C at 10 °C min^{-1} increments and holding for 30 min. A thermal conductivity detector (TCD) determined the amount of desorbed NH_3. Upon completion of each experiment, seven pulses of 5 mL of 10%NH_3/He were used to calibrate the TCD response. For 1-decene and/or DES + DBT mixture TPD experiments, conditions were kept identical to those described above, however, He was used as carrier gas throughout and the desired compounds were adsorbed on the catalyst rather than NH_3.

Identical TPD experiments were also performed using spent catalyst samples following reaction with 1-decene, DES and DBT, however no adsorption step was used.

TGA profiles were used to detect the desorption of chemisorbed species from Ag-Ga/ZSM-5 catalyst following pre-adsorption with DES and DBT. Pre-adsorption was achieved by placing 1 g of Ag-Ga/ZSM-5 catalyst into a solution of DBT dissolved in DBT (1:1 ratio by mass) and leaving in a sealed container overnight, the resultant catalyst sample was then dried in air at 80 °C for 2 h to remove any water. TGA measurements were undertaken with a simultaneous thermal analyser (PerkinElmer STA 6000). The sample was held at 50 °C for 1 min and then heated to 100 °C at a rate of 10 °C min^{-1} under 30 sccm N_2 flow, held for 30 min, heated to 330 °C, held for 10 min and finally ramped to 500 °C.

Surface area analysis was performed via N_2 physisorption analysis. The adsorption and desorption of N_2 on catalyst samples was measured using a Quadrosorb SI (Quantachrome Instruments). Samples were outgassed under vacuum at 350 °C overnight and brought to 77 K by immersion in a liquid N_2 bath. Total surface area was calculated using a multi-point BET analysis. Pore surface area and pore volumes were calculated using Barrett-Joyner-Halenda analysis. The *t*-plot method was used with the DeBoer model for the calculation of the statistical thickness to distinguish the contribution of micropores (<2 nm) to the total surface area.

TOF-SIMS was performed using a TRIFT V nano TOF (Physical Instruments) using a 30 keV Au+pulsed primary ion source in bunched mode. The TOF-SIMS analysis on all samples were collected over an area of 400 µm × 400 µm with a total ion dose <1012 $ions^{-1}$ cm^{-2}. Mass spectra were collected in the mass-to-charge range of 0–1850 *m/z*, for positive polarity and negative polarity. Charge compensation was accomplished using 10 eV electrons.

Computational calculations. DFT calculations were conducted by using DMol3 module in Materials Studio. B3LYP was selected as the exchange-correlation functional. The basis set DNP was used in the calculation. By using this basis set, the effect of occupied atomic orbital and valence atomic orbital have been considered and, a polarisation p-function on all hydrogen atoms was applied. Therefore, this basis set could provide reasonable accuracy with acceptable computational cost, which has been heavily used in DFT calculation for ZSM-5[51–53]. During geometry optimisation, the tolerances of energy, gradient and displacement convergence were 2×10^{-5} Ha, 4×10^{-3} Ha $Å^{-1}$ and 5×10^{-3} Å. The initial ZSM-5 structure was obtained from the database of International Zeolite Association (IZA-SC)[33, 54]. To conduct DFT calculation for non-periodic ZSM-5 cluster, the structure was hydrogen-terminated, which suggests all terminal Si and O atoms were saturated by hydrogen atom. During the geometry optimisation, the bond lengths of terminal O–H and Si–H were fixed at 0.95 Å and 1.49 Å, respectively. The initial structure has 96 T-sites. To satisfy a SiO_2/Al_2O_3 ratio of 23:1, 8 tetrahedral sites were replaced by Al atom. Based on the position of silicon atom, these T-sites can be classified into 12 groups, which were labelled from T1 to T12. Al atom is preferred located at T2 and T12 sites. To obey the aluminium avoidance principle, four T2 and T12 sites were occupied by Al[55]. The introduced Ag and Ga atom are located close to the Al to form [Al-O-M] (M = Ag, Ga) since metal atom has a preference to react with the Brønsted acid sites[56, 57].

Data availability

The data sets generated during and/or analysed during the current study are available from the corresponding author on reasonable request.

Received: 8 October 2018 Accepted: 7 March 2019
Published online: 25 March 2019

References

1. Shen, Y., Shuai, S., Wang, J. & Xiao, J. Optimization of gasoline hydrocarbon compositions for reducing exhaust emissions. *J. Environ. Sci.* **21**, 1208–1213 (2009).
2. Sawarkar, A. N., Pandit, A. B., Samant, S. D. & Joshi, J. B. Petroleum residue upgrading via delayed coking: a review. *Can. J. Chem. Eng.* **85**, 1–24 (2007).
3. Primo, A. & Garcia, H. Zeolites as catalysts in oil refining. *Chem. Soc. Rev.* **43**, 7548–7561 (2014).
4. Brunet, S., Mey, D., Pérot, G., Bouchy, C. & Diehl, F. On the hydrodesulfurization of FCC gasoline: A review. *Appl. Catal. A Gen.* **278**, 143–172 (2005).
5. Zhang, P., Guo, X., Guo, H. & Wang, X. Study of the performance of modified nano-scale ZSM-5 zeolite on olefins reduction in FCC gasoline. *J. Mol. Catal. A Chem.* **261**, 139–146 (2007).
6. Van Der Bij, H. E. & Weckhuysen, B. M. Phosphorus promotion and poisoning in zeolite-based materials: synthesis, characterisation and catalysis. *Chem. Soc. Rev.* **44**, 7406–7428 (2015).
7. Chen, N. Y., Kaeding, W. W. & Dwyer, F. G. Para-directed aromatic reactions over shape-selective molecular sieve zeolite catalysts. *J. Am. Chem. Soc.* **101**, 6783–6784 (1979).
8. Li, Y. et al. Aromatization and isomerization of 1-hexene over alkali-treated HZSM-5 zeolites: Improved reaction stability. *Appl. Catal. A Gen.* **338**, 100–113 (2008).
9. Rostrup-Nielsen, J. R., Sehested, J. & Nørskov, J. K. Hydrogen and synthesis gas by steam and CO_2 reforming. *Adv. Catal.* **47**, 65–139 (2002).
10. He, P., Lou, Y. & Song, H. Olefin upgrading under methane environment over Ag-Ga/ZSM-5 catalyst. *Fuel* **182**, 577–587 (2016).
11. He, P., Gatip, R., Yung, M., Zeng, H. & Song, H. Co-aromatization of olefin and methane over Ag-Ga/ZSM-5 catalyst at low temperature. *Appl. Catal. B Environ.* **211**, 275–288 (2017).
12. Lou, Y., He, P., Zhao, L. & Song, H. Refinery oil upgrading under methane environment over PdOx/H-ZSM-5: Highly selective olefin cyclization. *Fuel* **183**, 396–404 (2016).
13. Lou, Y., He, P., Zhao, L. & Song, H. Highly selective olefin hydrogenation: Refinery oil upgrading over bifunctional PdOx/H-ZSM-5 catalyst. *Catal. Commun.* **87**, 66–69 (2016).
14. He, P. et al. Selective participation of methane in olefin upgrading over Pd/ZSM-5 and Ir/ZSM-5: Investigation using deuterium enriched methane. *ChemistrySelect* **2**, 252–256 (2017).
15. Lou, Y., He, P., Zhao, L., Cheng, W. & Song, H. Olefin upgrading over Ir/ZSM-5 catalysts under methane environment. *Appl. Catal. B Environ.* **201**, 278–289 (2017).
16. Mashkina, A. V. & Khairulina, L. N. Catalytic reactions of dimethyl disulfide with thiophene and benzene. *Kinet. Catal.* **57**, 72–81 (2016).
17. He, P. et al. Co-aromatization of methane with olefins: the role of inner pore and external surface catalytic sites. *Appl. Catal. B Environ.* **234**, 234–246 (2018).
18. Bensebaa, F., Zhou, Y., Deslandes, Y., Kruus, E. & Ellis, T. XPS study of metal–sulfur bonds in metal–alkanethiolate materials. *Surf. Sci.* **405**, L472–L476 (1998).
19. Bird, R. J. & Swift, P. Energy calibration in the electron spectroscopy and the re-determination of some reference electron binding energies. *J. Electron Spectros. Relat. Phenom.* **21**, 227–240 (1980).
20. Jia, S., Wu, S. & Meng, Z. Study on the active center of Ga_2O_3/HZSM-5 catalyst. *Appl. Catal. A Gen.* **103**, 259–268 (1993).
21. Zepeda, T. A., Pawelec, B., Díaz de León, J. N., de los Reyes, J. A. & Olivas, A. Effect of gallium loading on the hydrodesulfurization activity of unsupported Ga_2S_3/WS_2 catalysts. *Appl. Catal. B Environ.* **111–112**, 10–19 (2012).
22. Lazell, M. R., O'Brien, P. O., Otway, D. J. & Park, J. Deposition of thin films of gallium sulfide from a novel single-source precursor, $Ga(S_2CNMeHex)_3$, by low-pressure metal-organic chemical vapor deposition. *Chem. Mater.* **11**, 3430–3432 (1999).
23. Armaleo, L., Colombo, P., Fabrizio, M., Gross, S. & Tondello, E. Sol-gel synthesis and characterization of Ag_2S nanocrystallites in silica thin film glasses. *J. Mater. Chem.* **9**, 2893–2898 (1999).
24. Thomas, J. M., Adams, I., Williams, R. H. & Barber, M. Valence band structures and core-electron energy levels in the monochalcogenides of gallium. *J. Chem. Soc. Faraday Trans. 2 Mol. Chem. Phys.* **68**, 755–764 (1972).
25. Nishi, K. et al. Deconvolution analysis of Ga K-Edge XANES for quantification of gallium coordinations in oxide environments. *J. Phys. Chem. B* **102**, 10190–10195 (1998).
26. Rane, N., Kersbulck, M., van Santen, R. A. & Hensen, E. J. M. Cracking of n-heptane over Brønsted acid sites and Lewis acid Ga sites in ZSM-5 zeolite. *Microporous Mesoporous Mater.* **110**, 279–291 (2008).
27. Jung, K., Chyi, A., Chung, H. & Fu, J. X-ray absorption spectroscopic study on the states of gallium and platinum in Pt/Ga/H-beta zeolites. *Microporous Mesoporous Mater.* **36**, 413–424 (2000).
28. Cini, M. Ionization potentials and electron affinities of metal clusters. *J. Catal.* **37**, 187–190 (1975).
29. Gómez, B. & Martińez-Magadán, J. M. A theoretical study of dibenzothiophene absorbed on open-ended carbon nanotubes. *J. Phys. Chem. B* **109**, 14868–14875 (2005).
30. De Klerk, A. Oligomerization of 1-hexene and 1-octene over solid acid catalysts. *Ind. Eng. Chem. Res.* **44**, 3887–3893 (2005).
31. Qiu, P., Lunsford, J. H. & Rosynek, M. P. Characterization of Ga/ZSM-5 for the catalytic aromatization of dilute ethylene streams. *Catal. Lett.* **52**, 37–42 (1998).
32. Van De Voorde, B. et al. Adsorptive desulfurization with CPO-27/MOF-74: An experimental and computational investigation. *Phys. Chem. Chem. Phys.* **17**, 10759–10766 (2015).
33. Olson, D. H., Kokotailo, G. T., Lawton, S. L. & Meier, W. M. Crystal structure and structure-related properties of ZSM-5. *J. Phys. Chem.* **85**, 2238–2243 (1981).
34. Kazansky, V. B. The nature of adsorbed carbenium ions as active intermediates in catalysis by solid acids. *Acc. Chem. Res.* **24**, 379–383 (1991).

35. Boronat, M., Viruela, P. & Corma, A. Theoretical study of the mechanism of zeolite-catalyzed isomerization reactions of linear butenes. *J. Phys. Chem. A* **102**, 982–989 (1998).
36. Kazansky, V. B. Adsorbed carbocations as transition states in heterogeneous acid catalyzed transformations of hydrocarbons. *Catal. Today* **51**, 419–434 (1999).
37. Buchanan, J. S., Santiesteban, J. G. & Haag, W. O. Mechanistic considerations in acid-catalyzed cracking of olefins. *J. Catal.* **158**, 279–287 (1996).
38. Guisnet, M. & Magnoux, P. Deactivation by coking of zeolite catalysts. Prevention of deactivation. Optimal conditions for regeneration. *Catal. Today* **36**, 477–483 (1997).
39. Guisnet, M. & Gnep, N. S. Aromatization of propane over GaHMFI catalysts. Reaction scheme, nature of the dehydrogenating species and mode of coke formation. *Catal. Today* **31**, 275–292 (1996).
40. Lukyanov, D. B., Gnep, N. S. & Guisnet, M. R. Kinetic modeling of propane aromatization reaction over HZSM-5 and GaHZSM-5. *Ind. Eng. Chem. Res.* **34**, 516–523 (1995).
41. Kim, K. et al. Lanthanum-catalysed synthesis of microporous 3D graphene-like carbons in a zeolite template. *Nature* **535**, 131–135 (2016).
42. Ogura, M. et al. Alkali-treatment technique - New method for modification of structural and acid-catalytic properties of ZSM-5 zeolites. *Appl. Catal. A Gen.* **219**, 33–43 (2001).
43. Groen, J. C. et al. Direct demonstration of enhanced diffusion in mesoporous ZSM-5 zeolite obtained via controlled desilication. *J. Am. Chem. Soc.* **129**, 355–360 (2007).
44. Groen, J. C., Moulijn, J. A. & Pérez-Ramírez, J. Desilication: on the controlled generation of mesoporosity in MFI zeolites. *J. Mater. Chem.* **16**, 2121–2131 (2006).
45. Dapsens, P. Y., Mondelli, C. & Pérez-Ramírez, J. Highly selective Lewis acid sites in desilicated MFI zeolites for dihydroxyacetone isomerization to lactic acid. *ChemSusChem* **6**, 831–839 (2013).
46. Eberly, P. E. High-temperature infrared spectroscopy of pyridine adsorbed on faujasites. *J. Phys. Chem.* **71**, 1717–1722 (1967).
47. Emeis, C. A. Determination of integrated molar extinction coefficients for infrared absorption bands of pyridine adsorbed on solid acid catalysts. *J. Catal.* **141**, 347–354 (1993).
48. Hsieh, M. F., Zhou, Y., Thirumalai, H., Grabow, L. C. & Rimer, J. D. Silver-promoted dehydroaromatization of ethylene over ZSM-5 catalysts. *ChemCatChem* **9**, 1675–1682 (2017).
49. Gabrienko, A. A. et al. Methane activation and transformation on Ag/H-ZSM-5 zeolite studied with solid-state NMR. *J. Phys. Chem. C* **117**, 7690–7702 (2013).
50. Luzgin, M. V. et al. The 'alkyl' and 'carbenium' pathways of methane activation on Ga-modified zeolite BEA: ^{13}C solid-state NMR and GC-MS study of methane aromatization in the presence of higher alkane. *J. Phys. Chem. C* **114**, 21555–21561 (2010).
51. Gao, J. et al. Spectroscopic and computational study of Cr oxide structures and their anchoring sites on ZSM-5 zeolites. *ACS Catal.* **5**, 3078–3092 (2015).
52. Arvidsson, A. A., Zhdanov, V. P., Carlsson, P. A., Grönbeck, H. & Hellman, A. Metal dimer sites in ZSM-5 zeolite for methane-to-methanol conversion from first-principles kinetic modelling: Is the $[Cu\text{-}O\text{-}Cu]^{2+}$ motif relevant for Ni, Co, Fe, Ag, and Au? *Catal. Sci. Technol.* **7**, 1470–1477 (2017).
53. Huang, Y., Dong, X., Li, M. & Yu, Y. A density functional theory study on ethylene formation and conversion over P modified ZSM-5. *Catal. Sci. Technol.* **5**, 1093–1105 (2015).
54. Kokotailo, G. T., Lawton, S. L., Olson, D. H. & Meier, W. M. Structure of synthetic zeolite ZSM-5. *Nature* **272**, 437–438 (1978).
55. Fripiat, J. G., Berger-André, F., André, J. M. & Derouanc, E. G. Non-empirical quantum mechanical calculations on pentasil-type zeolites. *Zeolites* **3**, 306–310 (1983).
56. Pidko, E. A., Kazansky, V. B., Hensen, E. J. M. & van Santen, R. A. A comprehensive density functional theory study of ethane dehydrogenation over reduced extra-framework gallium species in ZSM-5 zeolite. *J. Catal.* **240**, 73–84 (2006).
57. Gonzales, N. O., Chakraborty, A. K. & Bell, A. T. A density functional theory study of hydrogen recombination and hydrogen-deuterium exchange on Ga/H-ZSM-5. *Top. Catal.* **9**, 207–213 (1999).

Acknowledgements

The authors gratefully acknowledge the financial support from Alberta Innovates—Energy and Environment Solutions. We appreciate the XAS facilities provided by Taiwan Photon Source. The technical support from Dr. Lo Yueh Chang and TPS 44A beamline is acknowledged.

Author contributions

J.H.H. Performed the olefin upgrading reactions, catalyst characterisations, data analysis and wrote the paper. A.W. synthesised some of the catalysts and assisted with data analysis and catalyst characterisations. J.S.J. assisted with data analysis and paper writing. P.H. prepared some of the catalysts and performed XANES analysis. S.M. performed and analysed the DFT calculations. M.Y. performed N_2 physisorption analysis. L.L. assisted with XANES analysis. H.S. conceived the idea, directed the project and co-wrote the paper.

Additional information

Supplementary information accompanies this paper at https://doi.org/10.1038/s42004-019-0141-4.

Competing interests: The authors declare no competing interests.

Reprints and permission information is available online at http://npg.nature.com/reprintsandpermissions/

Publisher's note: Springer Nature remains neutral with regard to jurisdictional claims in published maps and institutional affiliations.